Seasonal asymmetries and long-term trends in atmospheric and ionospheric temperatures in polar regions and their dependence on solar activity (SATS)

Stein Haaland[1,2,3], Antonia Radlwimmer[3,4], Brandon van Schaik[5,6], Audrey Schillings[7], Lindis Bjoland[3,8]

1 Birkeland Centre for Space Science, Bergen, Norway
2 SEHS, Bern, Switzerland
3 The University Centre in Svalbard, Longyearbyen, Svalbard
4 University of Bonn, Bonn, Germany
5 Eindhoven University of Technology, Eindhoven, the Netherlands
6 École Polytechnique Fédérale de Lausanne, Lausanne, Switzerland
7 Department of Physics, Umeå University, Umeå, Sweden
8 Space Plasma Physics Group, University of Bergen, Bergen, Norway

Corresponding author: Stein Haaland, Stein.Haaland@uib.no
ORCID number: 0000-0002-1241-7570

Keywords: Temperatures, seasonal asymmetry, atmosphere, mesosphere, ionosphere, solar activity

DOI: https://doi.org/10.5281/zenodo.7371477

1. Introduction

Solar radiation is fundamental for all life on Earth. Radiation in the infrared and visible part of the solar spectrum is more or less constant over time. In the ultraviolet (UV) range, and in particular in the extreme ultraviolet (EUV) range, however, there are significant variations, which largely follow the solar cycle with its 11-year period. This UV radiation ionises parts of the upper atmosphere, and an electrically conductive layer – the ionosphere – is formed at a height of 100-300 km. Since UV radiation only constitutes a small fraction of the total radiation, the total variation in solar irradiance, and thus the variation in radiation energy from the Sun is only about 0.1% over the solar cycle (Coddington et al. 2019).

Around vernal and autumnal equinoxes, the incoming solar radiation is nearly identical for both hemispheres. The local temperature at a given altitude, however, is strongly influenced by local conditions. Landmasses (including glaciers) and water (sea) have large heat capacities, and energy transport in the form of wind and ocean currents cause large local variations on different timescales. Still, it is usually much warmer, in the sea, on land, and in the atmosphere during autumnal equinox than vernal equinox: there is a seasonal asymmetry in temperatures on ground.

Such seasonal asymmetries are strongest at high latitudes. In Svalbard, average temperatures around vernal equinox (March) can be as much as 15 degrees lower than at autumnal (September) equinox, and the yearly maximum temperature typically occurs almost 50 days after solstice as illustrated in Figure 1. At higher altitudes in the atmosphere, where the heat capacity of land or sea is less important, the seasonal asymmetry is expected to be smaller.

Somewhat surprisingly, similar seasonal asymmetries in temperatures have also been detected in space. Specifically, plasma temperatures inferred from EISCAT Svalbard radar measurements and observations from satellite measurements in the high latitude ionosphere at 200-400 km altitudes have shown such asymmetries (Aruliah et al. 1996; Hatch et al. 2020). There are also indications that such asymmetries exist in the magnetosphere (Haaland et al. 2017).

In space, electromagnetic forces play a key role for the temperature and motion of gases. Much of the dynamics, including transport and heating, is driven by the interaction between the solar wind and the Earth's magnetic field. In particular, solar activity and the orientation of the interplanetary magnetic field play crucial roles. Measurements from satellites (Förster et al. 2008) indicate that the motion of plasma in space also influences the neutral atmosphere, and sets up circulation and redistribution of energy in the upper atmosphere. This effect is most pronounced at high latitudes where the magnetic field is directly coupled to the interplanetary space.

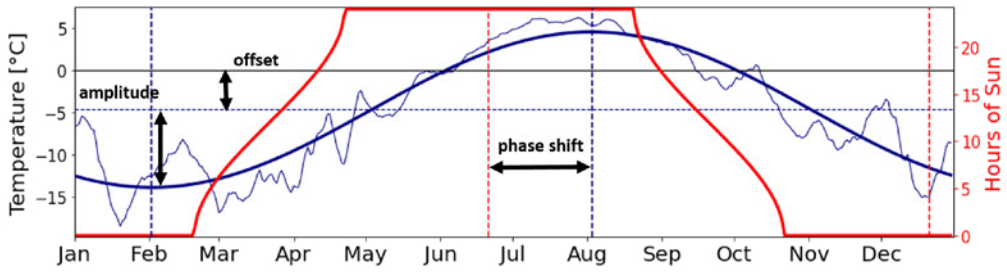

Figure 1: Illustration of temperature asymmetry at Ny-Ålesund airport. The ragged blue line shows the daily median temperature (smoothed with a 7-day rolling window) as a function of season based on daily averages between 2000 and 2002. The solid blue curve is a model fit to the measurements, using a simple sinusoidal variation as the model. The red curve shows the corresponding number of daylight hours. We quantify the seasonal asymmetry as the **phase shift** (in number of days) between solar illumination maximum (at solstice) and the maximum temperature of the fitted curve (early August). **Amplitude** is defined as the difference between lowest and highest temperatures of the model fit, and **offset** is the difference between the yearly average model temperature and 0°C.

Conversely, transport of neutral material due to thermal effects may also affect plasma motions in the ionosphere and even the magnetosphere. Since the atmosphere is the prime supplier of plasma to the magnetosphere (through a process called ionospheric outflow), the seasonal asymmetry can have a profound effect on supply of plasma to the magnetosphere, and thus space weather phenomena such as geomagnetic substorms and auroral activity. This cross-coupling between the atmosphere and space is still poorly understood, partly because it spans two science disciplines: space science and atmospheric science.

In this report, we have used measurements from a number of observations in and above Svalbard (see Figure 2) to study how the temperature asymmetry varies with altitude, and whether this asymmetry has changed over time. We also investigated whether a relation (possibly cause/effect) exists between solar activity and temperatures in the sea, on ground, and in the atmosphere.

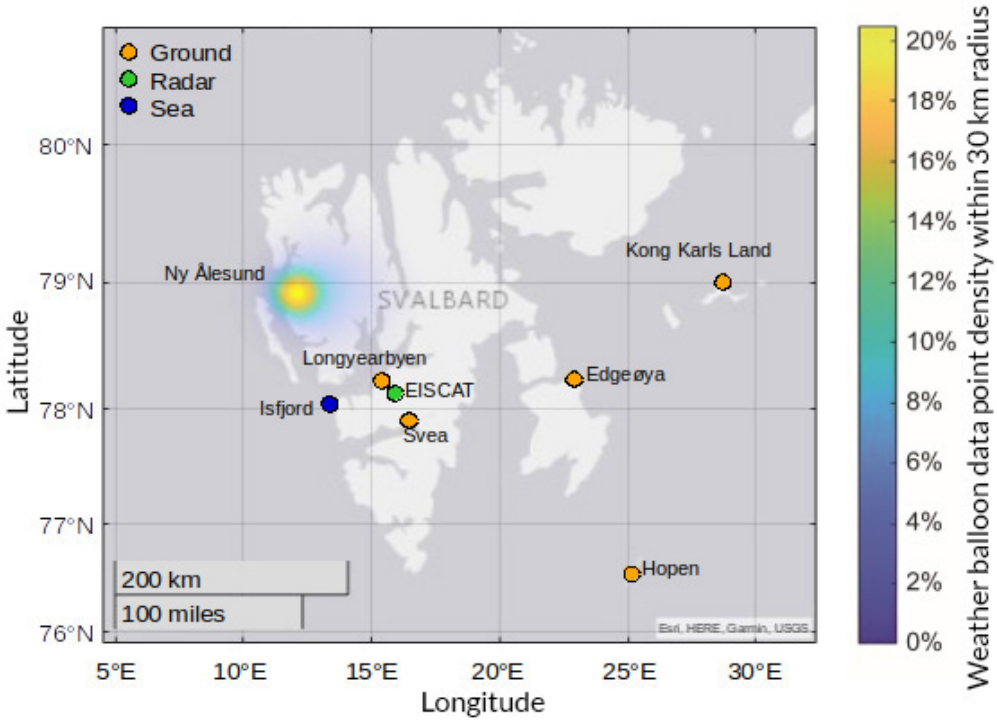

Figure 2: Map of ground stations with temperature measurements (yellow circles), the EISCAT Svalbard radar (green) and the mouth of Isfjorden where sea temperatures have been measured (blue). Balloon measurements are obtained from Ny-Ålesund, and the horizontal spread of the balloons as they rise is indicated as a colour-coded cloud.

2. Data and methodology

Tables 1 and 2 and the map in Figure 2 provide an overview of observatories, their location and availability of data used for this study. In the following subsections we briefly describe the data sources and methodology used.

A note about temperatures and units: traditionally, temperatures are given either as absolute temperatures in units of Kelvin – hereafter denoted [K], or in degrees Celsius [°C]. The freezing point of water (0°C) is equivalent to 273.15 K, with a temperature difference of 1°C equivalent to a difference of 1 K, meaning the unit size in each scale is the same.

2.1. Svalbard Sea temperatures

For the present study, we had access to a limited set of measurements of ocean temperatures obtained from buoys deployed at various depths from ships

near the mouth of Isfjorden (Skogseth et al. 2020). Measurements exist for the period September 2005 until August 2018, but with intermittent data gaps. Notably, there are no data between February 2008 and August 2010.

Table 1: List of observatories, their geographic location and elevation, time of operation and data availability.

Station	Lat [°]	Lon [°]	Alt [m]	Time period	Number of records	Tavg
Isfjord mouth	78.06	13.52	≥ -210	2005-09-16 - 2021-10-08	95969	3.0 °C
Hopen (HOP)	76.51	25.01	6	1970-01-01 - 2022-05-04	19098	-1.9 °C
Ny-Ålesund (NAL)	78.92	11.89	8	1974-08-01 - 2022-06-16	17146	-3.5 °C
Longyearbyen Airport (LYR)	78.24	15.49	9	1975-08-01 - 2022-06-16	17037	-3.1 °C
Svea (SVE)	77.89	17.72	9	1978-05-01 - 2022-05-04	15422	-3.8 °C
Edgeøya (EDG)	78.25	22.81	14	2006-01-11 - 2022-06-16	4797	-3.7 °C
Kong Karl VII øya (KXI)	78.92	28.72	5	2006-03-02 - 2022-06-13	3111	-3.1 °C
Mesosphere (nightglow)	78.15	16.04	ca 90km	1980-12-08 - 2022-02-27	2198	207.3 K **(1)**
Mesosphere (radar)	78.17	16.00	ca 90km	2001-10-16 - 2022-06-12	6679	181.1 K **(2)**
EISCAT Svalbard	78.09	16.03	**(3)**	1999-12-01 - 2021-03-23	4837	486.0 K

(1) During the dark season only, thus different averages from radar (2) measurements, from which measurements are available throughout the year. (3) EISCAT provides height profiles of plasma parameters. Depending on programme, the range can be from 100 to 1200 km. See Section 2.5 for more details.

2.2. Ground based temperatures

For near surface atmospheric temperatures, we find a wealth of observations in the region, dating back several decades. The stations chosen for this study are maintained by the Norwegian Meteorological Institute and listed in Table 1. Each station is presently equipped with a PT100 temperature sensor (standard for all MET Norway stations), succeeding manual readings taken for 2000 sec every 6 hours. As our research interest lies with seasonal patterns and long-time trends, daily means provide sufficient temporal resolution. Where possible, these means are given as the arithmetic mean of 24-hourly observations. However, before the early 21st century hourly observations are often unavailable. Here, the mean is taken from fewer, manual daily readings. The temperatures are measured at a default height of 2 m above ground.

All near surface atmospheric temperature data used in this study are taken from MET Norway's services. We downloaded the daily mean air temperatures directly from the Norwegian Centre for Climate Services[1].

2.3. Atmospheric weather balloon data

The temperature of the atmosphere can be directly measured with fast-response temperature sensors

1 https://seklima.met.no/

on weather balloons. The Norwegian Meteorological Institute and Alfred Wegner Institute have been collecting empirical temperature data from the lower atmosphere (0-40 km) at Ny-Ålesund on a daily basis since 1 January 1993. From this location, weather balloons are launched in fixed time frames, 09:00, 12:00 and 16:00 UTC, and the balloons rise with a rate of approximately 5 m/s.

We have calculated aggregate values at various pressure levels (isobars) as shown in Table 2. Since the pressure varies exponentially, and the height ranges are given in metres, the number of samples varies greatly between the isobars.

Since the weather balloon data are intermittent in time, microwave radiometer measurements from Ny-Ålesund, collected since January 2018 by the German Meteorological Institute, are used to identify daily fluctuations in temperatures. This analysis shows that the daily fluctuations are negligible with respect to temperature variations that are observed at altitude. Therefore, the time of day is disregarded and all data points can be averaged on a daily basis without correction.

Moreover, weather balloon data tends to vary in location during flight due to horizontal motion caused by winds. In Figure 2, the data point density of the weather balloon data is plotted as a heat map over Svalbard. Since the majority of data are taken within 15 km of the launch site, we disregard the effects of horizontal motion.

Table 2: Aggregate values from weather balloon observations from Ny-Ålesund (78.92 N, 11.89 E) at 11 different pressure heights between ground (pressure level 1000) to the upper stratosphere (pressure level below 100 hPa).

Pressure level [hPa]	Average height [m]	Number of records	Tavg [°C]
1000	75	54507	-2.4
900 - 1000	500	527903	-5.2
800 - 900	1,375	735815	-9.8
700 - 800	2,325	651119	-13.9
600 - 700	3,400	724818	-19.7
500 - 600	4,625	833663	-27.3
400 - 500	6,050	975353	-36.8
300 - 400	7,775	1205420	-48.1
200 - 300	9,873	1566151	-53.5
100 - 200	13,550	2531448	-51.8
0 - 100	22,900	7156433	-52.6

2.4. Mesospheric temperatures

We have used two different data sets for the temperatures near the mesopause. The first data set contains data from 1980 and estimates mesospheric temperatures from the spectral emissions of the excited hydroxyl (OH*), commonly called nightglow.

Hydroxyl emissions are taken at approximately 90 km altitude for an area of approximately 9 km to 12 km, using a Ebert-Fastie spectrometer currently located at the KHO, Longyearbyen (Sigernes et al. 2003). Until 2007, the spectrometer was located at the auroral station in Adventdalen. At high latitude, the nighttime OH* layer is directly proportional to the atomic oxygen concentration (Grygalashvyly 2015), thus we observe the OH* layer with the lowest altitudes and highest number densities during the winter.

The second data set consists of temperatures derived from daily echoes caused by ablation of meteors in the mesosphere (Hocking et al. 1997) using he Nippon/Norway Svalbard Meteor Radar, located in Adventdalen (Hall et al. 2002). This technique uses the ambipolar diffusion coefficient from the plasma trail formed by a meteor while

entering the atmosphere. Unlike the nightglow technique, radar measurements are available throughout the year. Measurements are available since 2001.

Both data sets, calculations and instrumentation are well described in Holmen (2016), and we refer to this thesis for details. Mesospheric temperature derivations are subject to larger uncertainties than ground-based or balloon-based temperatures. Still, these derived temperatures provide information in an altitude range too high for weather balloons and below the altitude of satellites.

2.5. Ionospheric temperatures

The European Incoherent SCatter Radar (EISCAT) in Svalbard (Folkestad et al. 1983; Maeda et al. 2002) provides height profiles of plasma temperatures (electron and ion temperatures) from approximately 100 km to ca 1000 km altitude depending on the experiment. Below ca 300 km, the ion temperature can be used as an approximation for the neutral temperature (Brekke 1993).

Note that EISCAT does not provide continuous data; measurements are typically taken during campaigns. The best data coverage was obtained during the international geophysical year (2007-2008). In this study, we use a specially prepared data set consisting of daily EISCAT temperatures from the fixed direction 42 m antenna for local noon.

2.6. Solar activity and solar wind input energy

To investigate correlations and possible cause/effects between temperatures and solar conditions, we looked at two different parameters: solar illumination and solar wind electromagnetic energy coupling.

As a proxy for solar UV illumination and solar activity, we use the F10.7 index. This is a measure of the radio emissions at 10.7 cm wavelength, and has been measured every day at local noon at the Dominion Radio Astrophysical Observatory (DRAO) in Penticton, Canada, since 1947. It correlates well with sunspot numbers, and is often referred to when discussing solar activity; a high F10.7 index means high solar activity.

Additionally, we estimated the solar energy input (similar to Poynting flux) to the Earth's magnetosphere derived from the solar wind parameters. This is the amount of electromagnetic energy transferred from the solar wind into the Earth's magnetosphere. Based on the original Vasyliunas formula (Vasyliunas et al. 1982), a later paper by Tenfjord and Østgaard (2013) proposed the following formula to quantify solar wind electromagnetic energy input for long time series:

$$P_{input}[W] = \frac{M_A \cdot V_{SW,x} \cdot B_T^2}{\mu_0} \cdot \sin\left(\frac{\theta}{2}\right)^4 \frac{167}{5 \cdot 10^{22} |B_z|^3 + 1} R_E^2 \quad (1)$$

where M_A is the solar wind Alfvèn Mach number, $\mu_0 = 4\pi \times 10^{-7}$ [kg m A^{-2} s^{-2}] the vacuum permeability, $V_{SW,x}$ [m s^{-1}] the solar wind velocity, $B_T = \sqrt{B_Y^2 + B_Z^2}$ [T] the transverse component of the interplanetary magnetic field (IMF), θ [rad] the clock angle and $\frac{167}{5 \cdot 10^{22} |B_z|^3 + 1} R_E^2$ is the effective area in which the solar wind interacts with the Earth's magnetosphere (R_E = Earth radius = 6371 km).

2.7. Estimation of seasonal asymmetry

In order to coherently quantify the seasonal temperature asymmetries at all altitudes, a relative measure of the seasonal temperature cycle is needed. Hence, where data availability allowed, a sinusoidal model was fitted to the observations as follows:

$$T = A \cdot sin\left(\frac{2\pi}{365.242} \cdot (t - 81) - B\right) + C \quad (2)$$

where $T = T(t)$ is the temperature [K] as a function of time, with fit parameters **A the amplitude** [K], **B the phase shift** [days] and **C the temperature offset** [K] (see Figure 1). These fit parameters are used in the following as proxy for the characteristics of the annual temperature cycle. Note that the fitted sinusoidal model has a period of 365.242 days and that the ascending node through equilibrium position is set to the 81st day of the year. The 81st day of the year, somewhat unintuitively, does

not correspond to spring equinox. Instead, it was chosen for its position halfway between winter and summer solstice, which, as summer on the northern hemisphere is nine days longer than winter, is two days after spring equinox. The fitted phase shift can thus be thought of as spring time phase shift.

In the following, the fit is used on a five-year moving window, shifting by one year for each time step of the analysis. Thus, the fit parameters associated to a specific year resemble the parameters of the fit of five years, with the year in question at the centre. Five years was chosen to smooth out the more extreme fluctuations in any one year's seasonal cycle.

2.8. Caveats, statistical spreads and uncertainties in measurements and methodology

As with any collection of experimental data, there are uncertainties related to both measurements, methodology and the underlying assumptions. In terms of measurement accuracy, in-situ measurements (e.g. sea, ground, balloon temperature and solar wind measurements) are more accurate than derived temperatures e.g. mesospheric temperatures derived from radar or optical methods.

In this study, we also discuss averages, for example daily averages, which are based on a number of individual samples throughout the day. Consequently, there is a statistical spread in the measurements. Note that these spreads mainly reflect the genuine variability of nature, and should not be confused with uncertainty or error in the data. Statistical spread in the measurements is usually much larger than any measurement errors.

A challenge when assessing statistical spread in measurements based on several different methods is the role of sampling frequency and number of samples used to establish statistical moments. In the figures below, we therefore do not show error bars, as these would be misleading and strongly dominated by sample frequency and number of samples.

3. Results

Figure 3 shows the timeline of some of the key measurements used for this study. Already from this plot, variations on a number of time scales can be discerned. In the sea, on ground, and in the atmosphere, seasonal variations are dominating. These can be explained by the sinusoidal variation in the Earth's rotation axis throughout the year. The 11-year solar cycle (which is primarily an effect of the periodic polarity change Sun's intrinsic magnetic field) is also clearly discernible as modulations of the F10.7 index as shown in panel a) and the electromagnetic input energy (solar wind Poynting flux calculated using Equation 1) in panel b). Note that the electromagnetic input energy from the Sun lags the F10.7 index; The strongest solar wind–magnetosphere coupling takes place in the waning phase of the solar cycle, not during its peak.

Ionospheric temperatures (e.g. EISCAT ion temperatures shown in panel c) seem to be modulated by solar cycle variation. The other parameters, plotted in panels d) to g) possess strong seasonal variations (as well as diurnal variations, but as we use daily averages and focus on long term trends, these are ignored), and will be discussed in some detail below.

3.1. Seasonal asymmetry and trends in ground and atmospheric temperatures

We now discuss in more detail the parameters A - amplitude, B - phase shift (seasonal asymmetry), and C - offset as introduced above. These are derived from the model fit (Equation 2) applied to the various temperature measurements.

Figure 4 shows the evolution of the three key parameters (phase shift, amplitude, offset) for ground stations (left columns) during the last four decades, and for balloon measurements (right columns) since 1993. The coloured curves give the

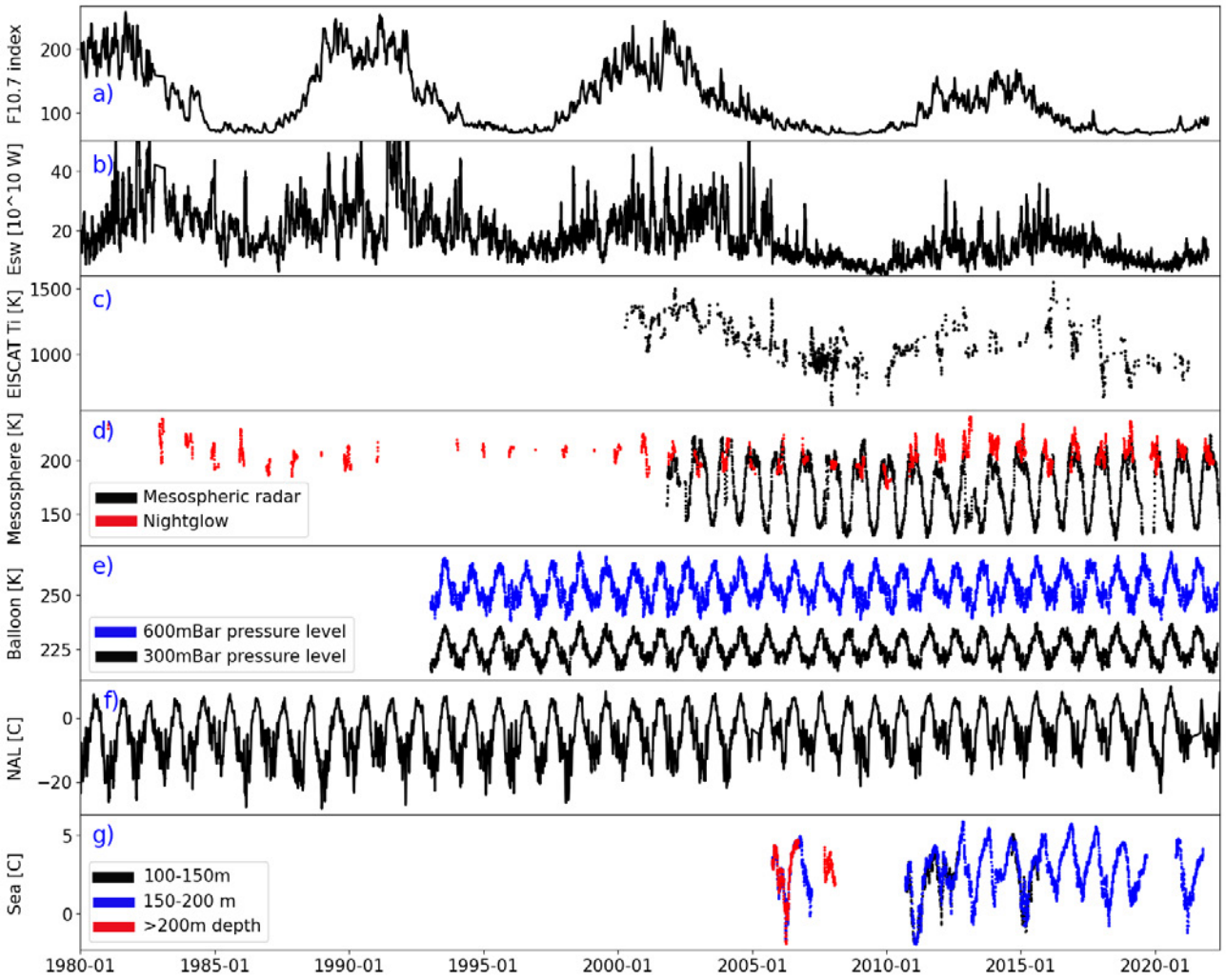

Figure 3: Timelines of some of the key measurements used for this study. Panel a) F10.7 index; b) Solar wind electromagnetic input energy (Poynting flux - see Equation 1); c) EISCAT ion temperatures; d) Mesospheric temperatures from radar (black solid lines) and nightglow observations (red dots, dark season only); e) Atmospheric temperatures at two altitudes (pressure levels) based on balloon measurements; f) Ground temperature [°C] from Ny-Ålesund airport (NAL); g) Sea temperatures [°C] from three different depth ranges in Isfjorden.

different ground stations, whereas the coloured dots represent different altitudes (or pressure levels) of the balloon measurements. We find several familiar traits: the signature of climate warming may be seen in the steady increase in temperature offset in the ground stations (panel e) over the last decades; the steady decrease of amplitude on ground (panel c) follows the warming of the winter months. For reference, we have also plotted the F10.7 index (panel g) for the same time period.

In terms of seasonal asymmetries, an increasing phase shift (panel a) can be observed from around 1990. Generally, all stations used exhibit a similar evolution of all three parameters. However, slight differences may be traced back to the local environments of the stations. Edgeøya (light blue curve) and Karl-XII-øya (dark blue curve), as islands on the east coast of Svalbard, are usually surrounded by sea ice for large portions of the year, leading to cooler mean temperatures. Svea (orange curve), which likewise is surrounded by ice in winter, is next coolest, while the stations on the ice-free west coast are warmest. In the phase shift the effect of ocean waters is also apparent. Stations located on smaller islands, e.g. Hopen (green curve), experience a greater phase shift. The pattern of the evolution of the phase shift parameter is difficult to interpret. There seems to be a diffuse oscillation signal. A possible cause is the yearly variation of sea ice extent. A quick crosscheck with the yearly minimum sea ice area (NASA[2]), however, did not seem promising.

2 https://climate.nasa.gov/vital-signs/arctic-sea-ice/

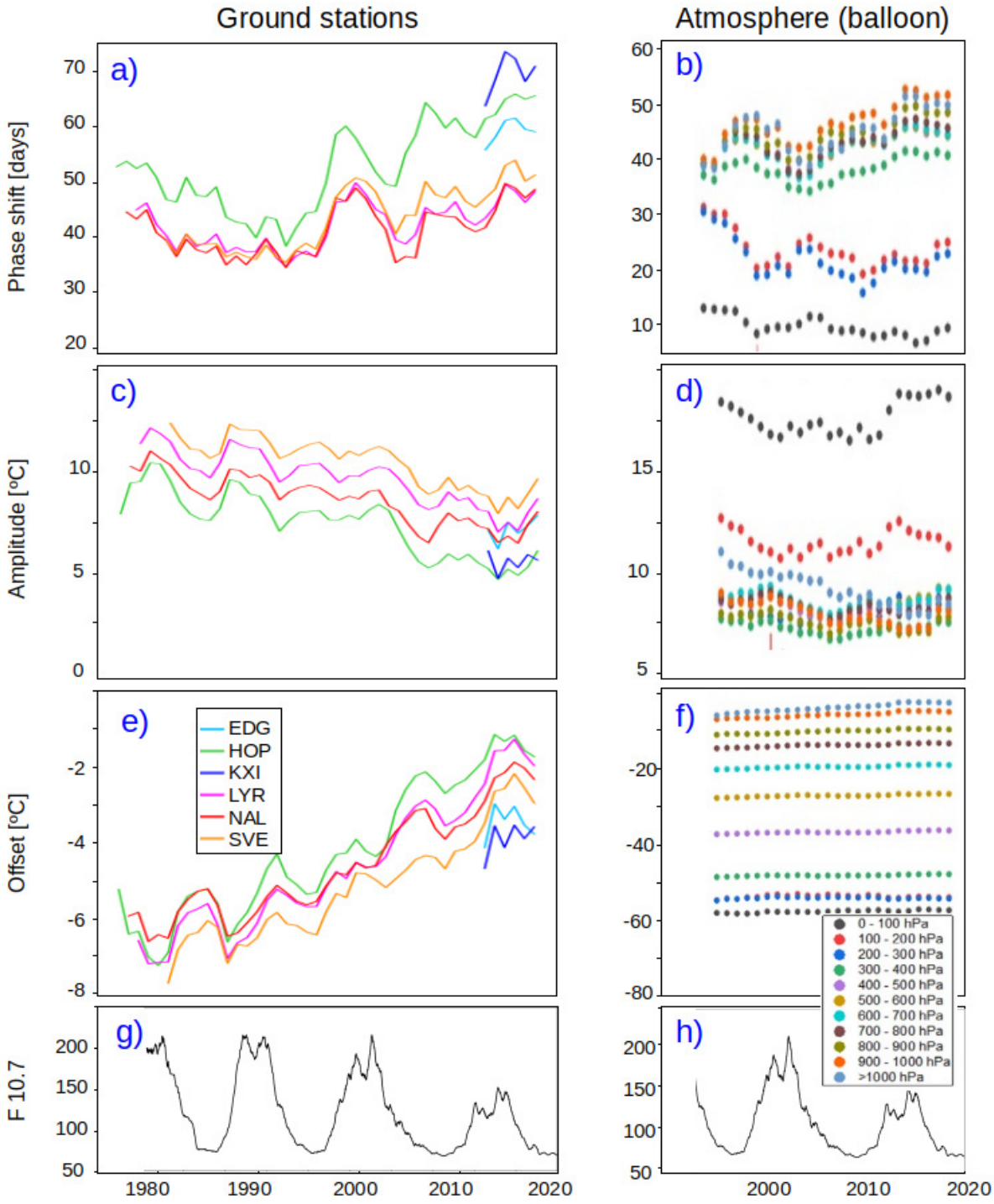

Figure 4: Evolution of key parameters on ground and in the atmosphere over the last decades. Panel a) Phase shift (seasonal shift) from ground stations; b) Phase shifts at various pressure altitudes derived from balloon measurements; c) Temperature amplitudes, ground stations; d) Temperature amplitudes from balloon measurements; e) Temperature offset, ground stations; f) Temperature offset, balloon measurements; g) F10.7 index for 1980-2020; h) F10.7 index for 1990-2020.

Atmospheric temperatures, derived from the balloon measurements (see Figure 4) generally show a similar evolution. Near ground (≥ 1000 hPa), the trends in phase shift (panel b) are similar to those derived from ground stations. Interestingly, the temporal variances in both the phase shift and the amplitude appear to be inverted for the high-altitude isobars (0-300 hPa) compared to lower altitudes. This phenomenon is likely caused by the absorption of UV radiation in this upper layer of air where more ozone is present (Randel and Wy 2010).

Moreover, much larger variances in the amplitude and phase shift can be observed in the ground station data compared to the lowest weather

balloon isobar. On average, these results should be equal; however, as there are more data points throughout the day for the ground stations, it is more likely that outliers will be observed, which explains why these parameters vary. It can furthermore be concluded that these short-term variances in amplitude and phase-shift cannot be observed in the weather balloon data due to insufficient number of data points to accurately map these outliers.

Figure 5 synthesises observations from the sea, ground, and atmosphere for more recent years. Each dot in this plot is the mean temperature over the years 2014-2021, i.e. when we have reasonable coverage from all observations. We once again note a significant phase shift (panel a) near the Earth's surface, suggesting that landmasses, glaciers and the ocean have a great impact on the local temperature. As we ascend further through the troposphere, this phase shift seems to reduce only slightly. However, as the tropopause is reached around the 200-300 hPa isobar (approximately 9 km altitude), there is a significant drop in the phase shift, and the phase shift eventually disappears completely vertical solid red line) at the highest balloon altitude, although a nearly half-year phase shift is observed in the mesosphere. Underwater (red dots and lines) the phase shift is amplified to greater temperature response lag, primarily due to the much larger heat capacity of water, though sea currents also probably play a role. The dotted line in the underwater phase shift indicates the lack of sufficient data points at pressures between12500 and 15000 hPa to enable an accurate fit.

In Panel b), which shows amplitude as function of pressure level, we observe a similar discrepancy between the troposphere and tropopause. The amplitude (i.e. average seasonal variation) does not vary significantly below the tropopause, whereas larger seasonal variations are seen above the tropopause, suggesting that the temperature is primarily modulated by solar irradiance. Below the sea surface, the temperature amplitude only varies a few degrees. Solar irradiation does not reach such depths underwater, and variations at these depths are primarily influenced by ocean currents. Panel c) shows the calculated offset. Being averages over several years, the offsets can be interpreted as the average temperature at that pressure level. A consistent decrease in the average temperature is observed as we move from underwater via ground and upwards through the troposphere. Above the tropopause (where pressure is below ca. 300 hPa), the temperature remains relatively constant.

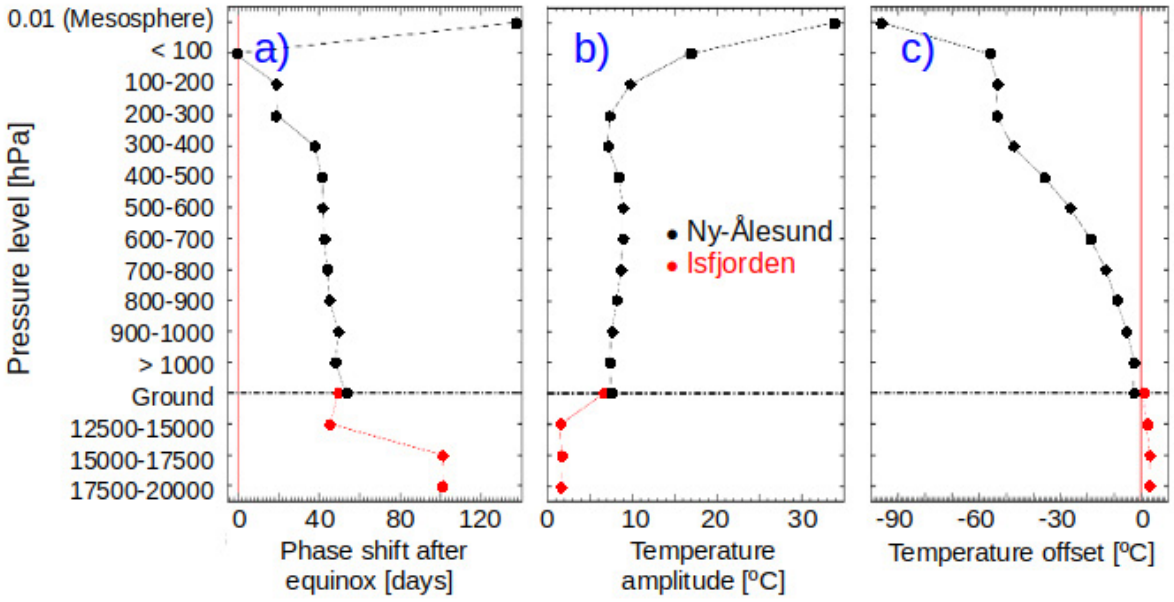

Figure 5: Fit parameters; a) Phase shift; b) Amplitude, and c) Temperature offset for various pressure levels in the atmosphere, ground (black lines and symbols) and under water (red), averaged between 2014-2021.

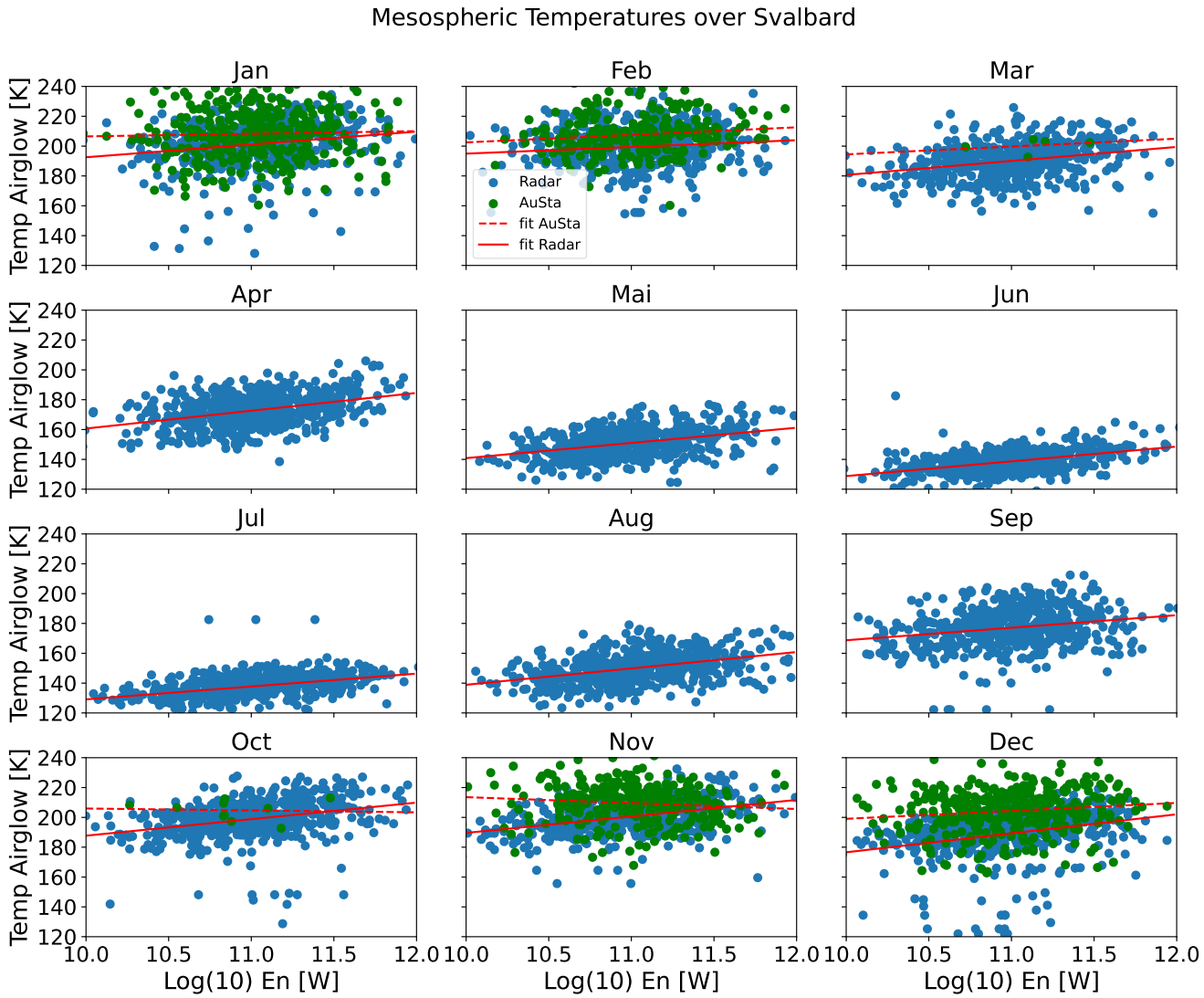

Figure 6: Monthly mesospheric temperatures between 1980 and 2021 as a function of the solar wind energy input in the Earth's magnetosphere. The temperatures are estimated at around 90 km derived from radar (blue dots) or spectrometer (green dots) measurements. Red lines represent a first-degree polynomial fitting for the spectrometer (dashed lines) and radar data (solid lines). Positive correlations, indicating a vertical coupling with some transfer of energy from the solar wind to the mesosphere, can be observed throughout the year.

3.2. Trends in the mesosphere and ionosphere and coupling to solar activity

Whereas the temperatures (and their trends) in the sea, on ground, and in the atmosphere do not show any clear correlation with solar activity or solar wind input, we do find a correlation between energy input and temperatures higher up. Figure 6 shows mesospheric temperatures as a function of the solar wind energy input (see Equation 1) for each month. Nightglow measurements (green dots) are only available during the dark season (late October to early March), whereas mesospheric temperatures derived from radar (blue dots) are available throughout the year. Despite some variability during the year, a general trend towards higher temperatures during periods with high solar wind energy input is seen for all months.

Figure 7 shows similar correlations, but this time between EISCAT measurements of ion temperatures around 300 km and the electromagnetic solar wind energy input. The correlation between the two parameters is even more pronounced. As noted above, around 300 km, neutral temperatures are on average very similar to ion temperatures.

Heating in the ionosphere can either be produced by Joule heating or through precipitation of soft electrons. The direct relation between the ion temperatures and Poynting flux has been shown by Banks and Kockarts (1973) at the altitude of the ionospheric E region (ca 90-150 km altitude) and lower F region (150-250 km). At higher altitudes, ion heating produced is sufficient to lead to direct ion outflow (Strangeway et al. 2000, 2005; Zheng et al. 2005).

3.3. Vertical coupling

In the mesosphere and above, a correlation between temperatures and electromagnetic energy from the Sun is observed, suggesting a vertical coupling and transfer of energy between regions. This coupling is most pronounced in ionospheric temperatures (Figure 7), where a clear correlation between solar activity and temperature can be observed. As shown in Figure 6, mesospheric temperatures are also correlated with the solar wind input energy, but the coupling is less pronounced than in the ionosphere.

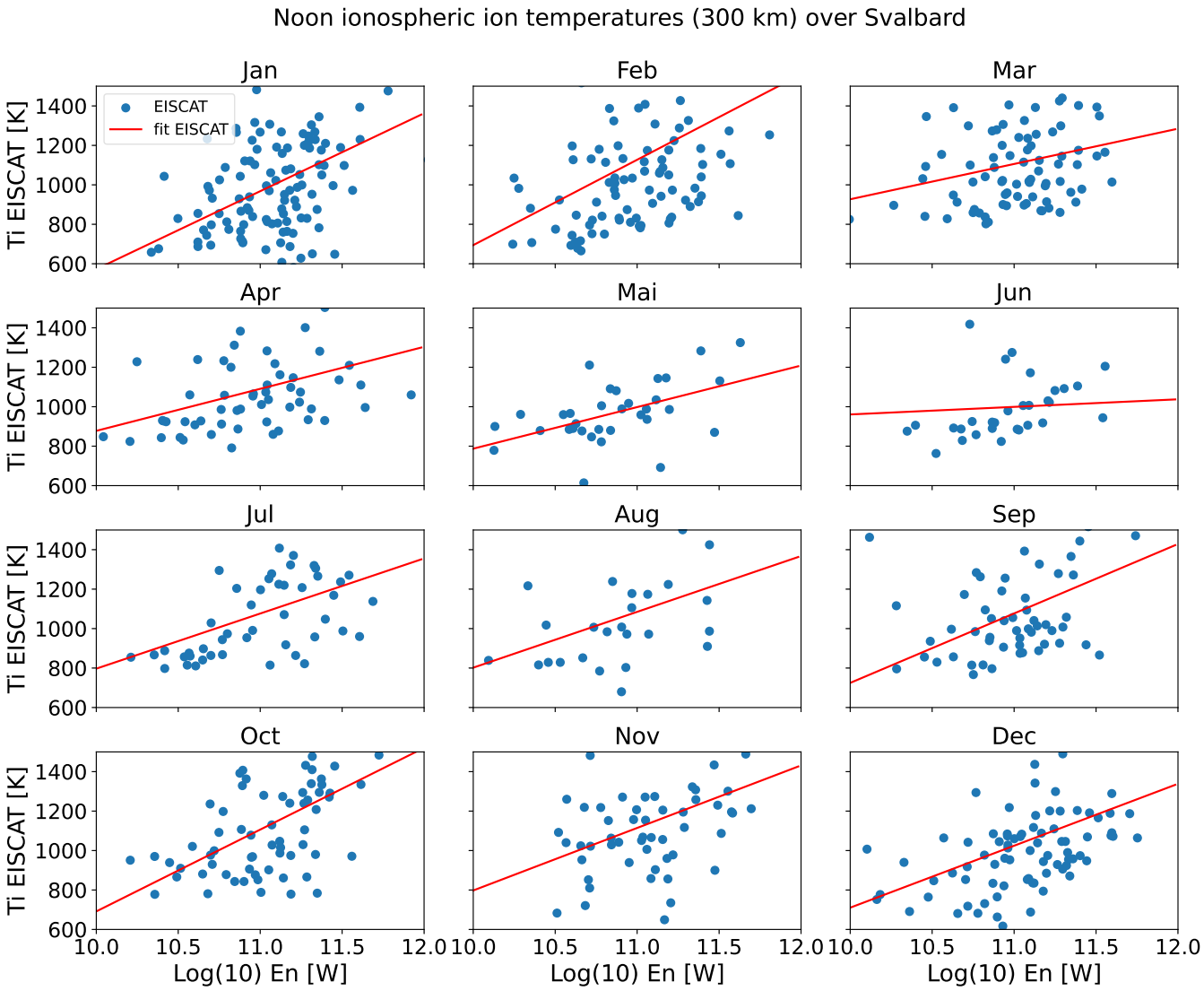

Figure 7: *Similar to figure 6, but now showing ionospheric ion temperatures at noon from EISCAT as a function of the solar wind energy input in the Earth's magnetosphere throughout the year. Solid red lines represent a first-degree polynomial fitting. Once again, there is a clear positive correlation between the solar wind input energy and ionospheric ion temperatures, indicating a transfer of energy from the solar wind to the ionosphere.*

Correlations between electromagnetic solar wind energy and the neutral atmosphere have been reported in earlier studies from high latitudes (Kosch and Nielsen 1995; Fujii et al. 1999). Such correlations have been attributed to Joule heating due to frictional forces between ions and neutrals (Cai et al. 2014), or heating due to small-scale field aligned currents (Lühr et al. 2004; Lühr and Marker 2013).

The former is related to enhanced ionospheric convection driven by solar wind–magnetosphere coupling through the so-called Dungey cycle (Dungey 1958). As a consequence, ions start moving faster than the neutrals. The resulting friction causes Joule heating. Signatures of field aligned currents in the thermosphere have been inferred from magnetic field measurements by the CHAMP satellites (Reigber et al. 2002), and one theory is that the Joule heating is caused by the combination of these fine structure currents and finite conductivity at 90-140 km altitude (Neubert and Christiansen 2003; Lühr et al. 2004).

Within the neutral atmosphere, at least below the tropopause, there is a strong vertical coupling where temperatures and their seasonal variation are correlated. Both diurnal and seasonal variations are observed, and these can be attributed to a combination of solar illumination and heat capacity in the sea, ground and ice/glaciers.

The existence of a direct coupling of solar wind input and the neutral atmosphere temperature cycles seems unlikely. If we calculate correlation coefficients between F10.7 and various ground stations, we note the values never exceed 0.25, and thus do not provide any convincing argument for direct relation between solar input and ground temperatures. Still, as shown in Figure 8, the evolution of the phase shift parameter from many ground stations bears an uncanny resemblance to that of the F10.7 parameter. The behaviour of the phase shift may be a coincidence, but this signal needs to be further explored in future studies.

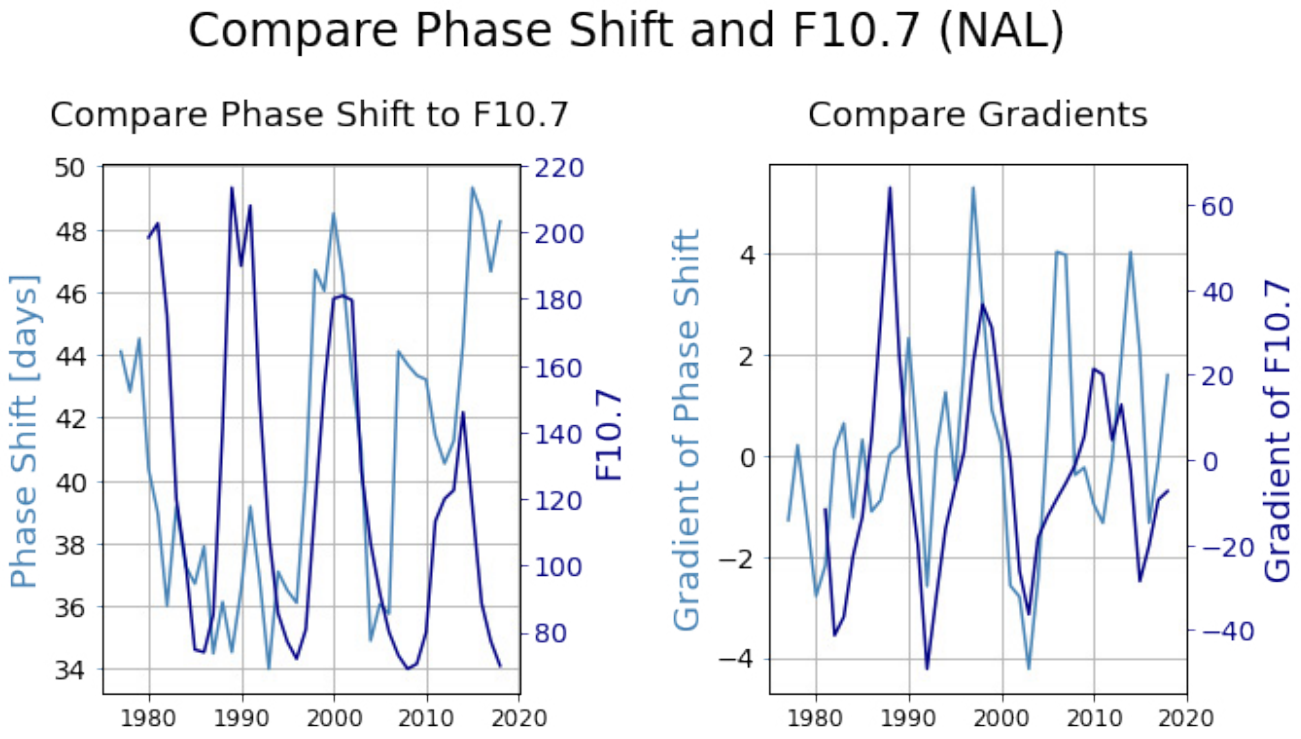

Figure 8: Left: Oscillation of phase shift in ground temperatures (with 5-year floating window), plotted with associated F10.7 values. Right: Gradients of self-same parameters. Data from Ny-Ålesund ground station.

4. Contributions to interdisciplinarity

We have studied long-term trends in temperatures in the sea, on ground, in the atmosphere in Svalbard, as well as the mesosphere and ionosphere above Svalbard. In particular, we have investigated how the seasonal asymmetry depends on altitude, and whether any of the trends observed can be explained by solar activity or enhanced energy transfer from the Sun and solar wind into the thermosphere.

The study spans several science disciplines: space physics, atmospheric physics, meteorology and oceanography. This interdisciplinarity implies some challenges. While the fundamental concepts such as temperature, density and convection are similar, forces responsible are very different in the different regions. Electromagnetic forces dominate in space, but are largely irrelevant on ground and in the atmosphere below the ionosphere. There are also practical challenges with data handling. In space, temperatures are frequently given in units of electronvolt [eV] or in K (Kelvin) whereas °C is more common in meteorology and oceanography. Still, the study has provided some interesting results, and new knowledge. Below we summarise the main results, list a couple of open questions and provide some recommendations for future utilisation of observations.

4.1. Main findings

The results of this study can be summarised as follows:

- On ground and in the lower atmosphere we observe a trend towards higher yearly average temperatures, and less difference between winter and summer temperatures. Over the ca 40 year time period considered, the difference in temperature between summer and winter has decreased about 2-3°C at the ground stations included in this study.
- We observe an increasing seasonal asymmetry between temperatures and season over the last decades; the day of the year with maximum temperatures tends to occur later in the year.
- While there is a significant phase shift between season and temperatures on ground and in the troposphere, there is little or no phase shift above the tropopause.
- We do not find any strong relation between the temperatures on ground or in the sea and solar activity.
- Likewise, there is little or no direct correlation between atmospheric temperatures and solar activity.
- In the higher parts of the thermosphere, in particular the ionosphere, but to some extent also the mesosphere, there is a pronounced correlation between solar input energy and temperatures.
- The most recently completed solar cycle, the 24th since systematic measurements started in 1755, shows a lower activity (lower EUV irradiance and electromagnetic energy transfer) than the earlier cycles for which we have reasonable data coverage. Despite this lower solar activity, the trend shows increased ground temperatures.

4.2. Open questions

While the study reveals some interesting trends and correlation between measurements from space, the atmosphere, the ground and the ocean, it also raises a couple of questions:

- What is the underlying reason for the observed trends? Is it primarily a result of global warming due to increased release of CO2 to the atmosphere, or are the observed trends primarily caused by local conditions and indirect effects, such as change of the ice-cap extent or ocean currents?
- Will the observed trends (as seen in e.g. Figure 4) continue in the coming years? An obvious follow-up question is: 'What consequences will these changes have in the future?'
- We do not observe any significant correlation between solar activity and ground temperatures. Does solar activity play any role for local temperatures in Arctic at all?

4.3. Recommendations for the future

With its extensive infrastructure, Svalbard is an ideal place to conduct studies focusing on the relation between solar activity on one side and processes and properties of the Earth's thermosphere on the other side. Still, this is a complex system involving several science disciplines. To enhance utilisation of data, we propose the following:

- Enhance cooperation between science disciplines: space science, meteorology, oceanography and glaciology. There are several conceivable ways to achieve this, for example by promoting cross-disciplinary study programs at universities, and by enhancing funding for cross-discipline and system science studies. Promoting common formats (such as netdcf, csv, cdf) within the disciplines could also facilitate interdisciplinary studies.
- Make sure measurements of critical parameters from space, from the atmosphere, from ground and in the sea/ice are available over extended epochs (ideally several solar cycles). Observations should ideally be continuous and without any major data gaps. In our study, we faced the measurements gap between highest altitude of atmospheric balloon (about 30 km) and the first altitude of EISCAT (about 80 km running on special Programme). The mesospheric measurements are very sporadic and not enough balloon data are available to make a feasible comparison with ground stations' data (see Section 3.1).
- Promote cross-disciplinary studies and modern data assimilation techniques like machine learning to identify couplings between processes.
- Continue to promote open access to observations, and make sure observations are well calibrated and contain sufficient metadata such as exact time and location of the observations, proper units, information about data gap handling and links to instrumentation papers with further details about the measurements and techniques.

5. Data availability

Data used for this study are available from public archives. Provider and Uniform Resource Locator (URL) is given in Appendix 1. See also Table 1 and 2 for details about location, parameters and time periods for the individual observations.

6. Acknowledgements

This work was supported by the Research Council of Norway, project number 322387, Svalbard Integrated Arctic Earth Observing System – Knowledge Centre, operational phase 2022. The authors also thanks staff and colleagues at the University Centre in Svalbard (UNIS), the Kjell Henriksen Observatory (KHO) and EISCAT for fruitful discussions and support in preparing this report. EISCAT is an international association supported by research organisations in China (CRIRP), Finland (SA), Japan (NIPR and ISEE), Norway (NFR), Sweden (VR), and the United Kingdom (UKRI).

7. References

Aruliah AL, Farmer AD, Fuller-Rowell TJ, Wild MN, Hapgood M, Rees D (1996) An equinoctial asymmetry in the high-latitude thermosphere and ionosphere. J Geophys Res: Space Physics 101:15713–15722. https://doi.org/10.1029/95JA01102

Banks PM, Kockarts G (1973) Aeronomy, Part B. Elsevier, New York.

Brekke A (1993) Physics of the Upper Atmosphere. Springer, Berlin, Heidelberg. https://doi.org/10.1007/978-3-642-27401-5

Cai L, Aikio AT, Nygrén T (2014) Solar wind effect on Joule heating in the high-latitude ionosphere. J Geophys Res: Space Physics 119 (10):440–10,455. https://doi.org/10.1002/2014JA020269

Coddington O, Lean J, Pilewskie P, Snow M, Richard E, Kopp G, Lindholm C, DeLand M, Marchenko S, Haberreiter M, Baranyi T (2019) Solar Irradiance Variability: Comparisons of Models and Measurements. Earth Space Sci 6:2525–2555. https://doi.org/10.1029/2019EA000693

Dungey JW (1958) Cosmic electrodynamics. Q J R Meteorolog Soc 85:450–450. https://doi.org/10.1002/qj.49708536628

Folkestad K, Hagfors T, Westerlund S (1983) EISCAT: An updated description of technical characteristics and operational capabilities. Radio Sci 18:867–879. https://doi.org/10.1029/RS018i006p00867

Förster M, Haaland SE, Rentz S, Liu H (2008) IMF Dependence of High-Latitude Thermospheric Wind Pattern Derived from CHAMP Cross-Track Accelerometer Data and the Corresponding Magnetospheric Convection from Cluster EDI Measurements. 37th COSPAR Scientific Assembly (Montreal, Canada)

Fujii R, Nozawa S, Buchert SC, Brekke A (1999) Statistical characteristics of electromagnetic energy transfer between the magnetosphere, the ionosphere, and the thermosphere. J Geophys Res: Space Physics 104:2357–2366. https://doi.org/10.1029/98JA02750

Grygalashvyly M (2015) Several notes on the OH* layer. Ann Geophys 33:923–930. https://doi.org/10.5194/angeo-33-923-2015

Haaland S, Lybekk B, Maes L, Laundal K, Pedersen A, Tenfjord P, Ohma A, Østgaard N, Reistad J, Snekvik K (2017) North-south asymmetries in cold plasma density in the magnetotail lobes: Cluster observations. J Geophys Res: Space Physics 122:136–149. https://doi.org/10.1002/2016JA023404

Hall CM, Aso T, Tsutsumi M (2002) An examination of high latitude upper mesosphere dynamic stability using the Nippon/Norway Svalbard Meteor Radar. Geophys Res Lett 29:1280. https://doi.org/10.1029/2001GL014229

Hatch SM, Haaland S, Laundal KM, Moretto T, Yau AW, Bjoland L, Reistad JP, Ohma A, Oksavik K (2020) Seasonal and Hemispheric Asymmetries of F Region Polar Cap Plasma Density: Swarm and CHAMP Observations. J Geophys Res 125:e28084. https://doi.org/10.1029/2020JA028084

Hocking WK, Thayaparan T, Jones J (1997) Meteor decay times and their use in determining a diagnostic mesospheric Temperature-pressure parameter: Methodology and one year of data. Geophys Res Lett 24:2977–2980. https://doi.org/https://doi.org/10.1029/97GL03048

Holmen SE (2016) Trends and variability of polar mesopause region temperatures attributed to atmospheric dynamics and solar activity. Dissertation, UiT - The Arctic University of Norway. https://munin.uit.no/handle/10037/10740

Kosch MJ, Nielsen E (1995) Coherent radar estimates of average high-latitude ionospheric Joule heating. J Geophys Res: Space Physics 100:12201–12216. https://doi.org/10.1029/95JA00821

Lühr H, Marker S (2013) High-Latitude Thermospheric Density and Wind Dependence on Solar and Magnetic Activity. In Lübken FJ (ed) Climate and Weather of the Sun-Earth System (CAWSES). Springer Atmospheric Sciences. Springer, Dordrecht, pp 189–205. https://doi.org/10.1007/978-94-007-4348-9_11

Lühr H, Rother M, Köhler W, Ritter P, Grunwaldt L (2004) Thermospheric up-welling in the cusp region: Evidence from CHAMP observations. Geophys Res Lett 31(6):L06805. https://doi.org/10.1029/2003GL019314

Maeda S, Nozawa S, Sugino M, Fujiwara H, Suzuki M (2002) Ion and neutral temperature distributions in the E-region observed by the EISCAT Tromsø and Svalbard radars. Ann Geophys 20:1415–1427. https://doi.org/10.5194/angeo-20-1415-2002

NASA's Jet Propulsion Laboratory, E S Arctic Sea Ice Minimum Extent. https://climate.nasa.gov/vital-signs/arctic-sea-ice/. Accessed 22 July 2022.

Neubert T, Christiansen F (2003) Small-scale, field-aligned currents at the top-side ionosphere. Geophys Res Lett 30:2010. https://doi.org/10.1029/2003GL017808

Randel WJ, Wu F (2010) The Polar Summer Tropopause Inversion Layer. J Atmos Sci 67:2572–2581. https://doi.org/10.1175/2010JAS3430.1

Reigber C, Lühr H, Schwintzer P (2002) CHAMP mission status. Adv Space Res 30:129–134. https://doi.org/10.1016/S0273-1177(02)00276-4

Sigernes F, Shumilov N, Deehr CS, Nielsen KP, Svenøe T, Havnes O (2003) Hydroxyl rotational temperature record from the auroral station in Adventdalen, Svalbard (78°N, 15°E). J Geophys Res: Space Physics 108(A9):1342. https://doi.org/10.1029/2001JA009023

Skogseth R, Olivier LL, Nilsen F, Falck E, Fraser N, Tverberg V, Ledang AB, Vader A, Jonassen MO, Søreide J, Cottier F, Berge J, Ivanov BV, Falk-Petersen S (2020) Variability and decadal trends in the Isfjorden (Svalbard) ocean climate and circulation - An indicator for climate change in the European Arctic. Prog Oceanogr 187:102394. https://doi.org/10.1016/j.pocean.2020.102394

Strangeway RJ, Russell CT, Carlson CW, McFadden JP, Ergun RE, Temerin M, Klumpar DM, Peterson WK, Moore TE (2000) Cusp field-aligned currents and ion outflows. J Geophys Res: Space Physics 105:21129-21141. https://doi.org/10.1029/2000JA900032

Strangeway R, Ergun R, Su Y-J, Carlson C, Elphic R (2005) Factors controlling ionospheric outflows as observed at intermediate altitudes. J Geophys Res: Space Physics 110: A03221. https://doi.org/10.1029/2004JA010829

Tenfjord P, Østgaard N (2013) Energy transfer and flow in the solar wind-magnetosphere-ionosphere system: A new coupling function. J Geophys Res: Space Physics, 118:5659–5672. https://doi.org/10.1002/jgra.50545

Vasyliunas VM, Kan JR, Siscoe GL, Akasofu S-I (1982) Scaling relations governing magnetospheric energy transfer. Planet Space Sci 30:359-365. https://doi.org/10.1016/0032-0633(82)90041-1

Zheng Y, Moore TE, Mozer FS, Russell CT, Strangeway RJ (2005) Polar study of ionospheric ion outflow versus energy input. J Geophys Res: Space Physics 110:A07210. https://doi.org/10.1029/2004JA010995

Appendix 1: Datasets used and their providers

Dataset	Provider and access (URL)	Data responsible / contact person for this SIOS project
Solar wind and solar indices	Coordinated Data Analysis Web, NASA, USA https://cdaweb.gsfc.nasa.gov/index.html Data description of the OMNI data set used for this study can be found on: https://cdaweb.gsfc.nasa.gov/misc/NotesO.html#OMNI_HRO_1MIN	Audrey Schillings, *Umeå University, Sweden* Audrey.Schillings@space.umu.se
EISCAT radar data	**EISCAT Scientific Association** http://pc115.seg20.nipr.ac.jp/www/eiscatdata/esr/ascii/42m_ascii/5min/	Lindis Bjoland, *UNIS, Svalbard* lindisb@unis.no
Atmospheric temperatures (balloon measurements)	Norwegian Meteorological Institute https://thredds.met.no/thredds/catalog/remotesensingradiosonde/catalog.html Alfred Wegener Institute, Germany: http://doi.pangaea.de/10.1594/PANGAEA.845373	Brandon van Schaik, b.j.a.v.schaik@student.tue.nl *École Polytechnique Fédérale de Lausanne, Switzerland*
Ground temperatures	Norwegian Centre for Climate Research https://www.seklima.met.no	Antonia Radlwimmer, UNIS, Svalbard Quivi@web.de
Ocean temperatures	Norwegian Polar Institute https://data.npolar.no/dataset/?filter-links.rel=data&q=Mooring	Lindis Bjoland, *Space Physics Group, University of Bergen* Lindis.Bjoland@uib.no